JREE: Vol. 12, No. 3, (Summer 2025) 21-35

Journal of Renewable Energy and Environment

Journal Homepage: www.jree.ir

Materials and Energy Research Center

MERC

Research Article

Effect of Working Fluids on the Performance of Ocean Thermal Energy Conversion Based Hybrid Systems Using Machine Learning Approach

Hadi Kamfar[a], Abolfazl Shojaeian[b]*, Jaber Yousefi Seyf[b], Najmeh Hajialigol[c]

[a] Department of Energy Engineering, Hamedan University of Technology, Hamedan, Iran.
[b] Department of Chemical Engineering, Hamedan University of Technology, Hamedan, Iran.
[c] Department of Mechanical Engineering, Hamedan University of Technology, Hamedan, Iran.

PAPER INFO

Paper history:
Received: 02 January 2025
Revised: 04 March 2025
Accepted: 15 June 2025

Keywords:
Thermal Efficiency,
Exergy Efficiency,
Working Fluids,
Machine Learning,
Ocean Thermal Energy Conversion

ABSTRACT

This study compares the performance of seven working fluids in hybrid ocean thermal energy conversion (OTEC) systems integrated with solar and wind energy. Plan B integrates thermoelectric technology with a wind turbine, while Plan C relies solely on a standalone wind turbine. Machine learning techniques were applied for performance prediction and multi-objective optimization. The results show that the R227ea working fluid achieves the highest power output and exergy efficiency—433.5 kW and 8.6% in Plan B, and 380.6 kW and 7.44% in Plan C, respectively. Conversely, the R125 working fluid exhibits the lowest performance, with an output power of 297.7 kW and an efficiency of 5.82% in Plan B, and 188.3 kW and 3.68% in Plan C. Additionally, Plan B outperforms Plan C across all performance metrics, including efficiency, power output, and cost-effectiveness, due to its hybrid configuration. Overall, the results demonstrate that optimal fluid selection (R227ea) and hybrid system design (Plan B) significantly enhance efficiency and cost-effectiveness, offering a practical pathway toward sustainable energy systems.

https://doi.org/10.30501/jree.2025.491739.2193

1. INTRODUCTION

The advancement of technology, coupled with population growth, is expected to exacerbate air pollution driven by continued reliance on fossil fuels. The ever-increasing demand for energy—fueled by both demographic expansion and technological progress—creates a vicious cycle that deepens this dependence. This reliance, compounded by inefficient energy practices, has led to a significant rise in air pollution. Harmful byproducts of fossil fuel combustion, such as sulfur dioxide, nitrogen oxides, and particulate matter, not only contribute to respiratory illnesses but also trigger a wide range of adverse health effects. Although technological innovation has improved energy efficiency, the current pace of change remains insufficient to counter the growing emissions of greenhouse gases. Chief among these is carbon dioxide, released through fossil fuel combustion, which traps heat in the atmosphere and drives global warming. The Earth's climate system is a complex web of interconnected processes, and the disruptions caused by rising temperatures are already affecting weather patterns, sea levels, and ecosystems on a global scale.

The severe consequences of continued fossil fuel use compel a re-evaluation of our energy choices. Transitioning to clean energy sources is no longer optional—it is an urgent necessity. Renewable energy options such as solar, wind, geothermal, and hydropower offer clean, abundant, and readily available alternatives to fossil fuels. Investment in research and development of advanced energy storage technologies and grid modernization will be critical to addressing the intermittency challenges associated with renewables. However, achieving a clean energy transition requires a coordinated global effort. Governments, industries, and individuals must collaborate to implement policies that incentivize renewable energy adoption, promote sustainable practices, and uphold long-term environmental stewardship. The world's commitment to addressing the climate crisis will directly shape the health and well-being of future generations (Li et al., 2023; Moradi CheshmehBeigi & Geravandi, 2023; Yang et al., 2024).

Therefore, countries around the world are actively seeking viable alternatives to fossil fuels and striving to reduce overall energy consumption. This global initiative is driven by the urgent need to mitigate the environmental and health impacts of fossil fuel use, as well as the economic and geopolitical risks associated with fossil fuel dependency. To diversify their energy portfolios and strengthen energy security, nations are investing in a range of renewable energy sources, including solar, wind, geothermal, and hydropower. Solar energy, with its vast potential and steadily declining costs, is being harnessed through both large-scale solar farms and rooftop photovoltaic installations. Wind energy—developed onshore and offshore—is expanding rapidly, capitalizing on the abundant wind resources available in many regions. Geothermal energy, which taps into the Earth's internal heat, provides a reliable and continuous source of power. Meanwhile, hydropower continues to serve as a foundational component of renewable

*Corresponding Author's Email: ab.shojaeian@gmail.com (A. Shojaeian)
URL: https://www.jree.ir/article_223267.html

Please cite this article as: Kamfar, H. , Shojaeian, A. , Yousefi Seyf, J. & Hajialigol, N. (2025). Effect of Working Fluids on the Performance of Ocean Thermal Energy Conversion Based Hybrid Systems Using Machine Learning Approach. *Journal of Renewable Energy and Environment (JREE)*, 12(3), 21-35. https://doi.org/10.30501/jree.2025.491739.2193

energy strategies in numerous countries (Geravandi & Moradi CheshmehBeigi, 2022; Mousavi et al., 2017; Zheng et al., 2024).

Due to its advantageous geographical location, Iran possesses substantial potential for harnessing renewable energy sources. The country's diverse natural resources—including the Caspian Sea, the Persian Gulf, abundant sunlight, and strong wind patterns—provide a robust foundation for the development of various renewable energy technologies. The Caspian Sea and the Persian Gulf, in particular, offer favorable conditions for ocean thermal energy conversion (OTEC) systems, which generate clean electricity by exploiting the temperature gradient between warm surface water and cold deep water. The consistent thermal differentials in these bodies of water make them ideal sites for OTEC plants, which can offer a reliable and sustainable source of energy. In addition to ocean thermal energy, Iran's significant solar potential represents another key asset. The country receives high levels of solar radiation, especially in its central and southern regions, making it well-suited for large-scale solar power development. Both photovoltaic (PV) systems and concentrated solar power (CSP) plants can be effectively deployed to capture and convert solar energy into electricity, thereby contributing to the national grid and reducing dependence on fossil fuels. Wind energy also holds considerable promise for Iran, particularly in regions characterized by strong and consistent wind flows. The northern and western parts of the country, as well as coastal areas along the Persian Gulf, are especially suitable for wind farm deployment. By installing wind turbines in these high-potential zones, Iran can harness wind power to produce clean electricity and further diversify its energy portfolio. Moreover, Iran's geographical features support the development of other renewable energy sources such as geothermal and hydropower. The country's mountainous terrain and volcanic activity offer opportunities for geothermal energy extraction, while its rivers and existing dam infrastructure provide the basis for hydropower generation. To fully realize its renewable energy potential, Iran must invest in research and development to enhance the efficiency and cost-effectiveness of these technologies. Collaboration with international partners and participation in global renewable energy initiatives could further accelerate the transition. Additionally, implementing supportive policies and incentives—such as feed-in tariffs, tax breaks, and streamlined permitting processes—will be critical to encouraging investment and innovation in the sector (Hoseinzadeh et al., 2024; Kannan & Vakeesan, 2016; Sahu, 2015).

Given the relatively small temperature difference between the cold and hot sources, the Ocean Thermal Energy Conversion (OTEC) system is inherently less efficient than conventional fossil fuel-based systems. Typically, the efficiency of OTEC systems ranges between 3% and 5% (Bernardoni et al., 2019; Yang & Yeh, 2014). To solve this problem and increase the efficiency of the OTEC system, methods such as selecting a suitable working fluid (Abbas et al., 2023; Ahmadi et al., 2013; Chen & Huo, 2023; Khosravi et al., 2019; Soto & Vergara, 2014; Wu et al., 2019), combining the OTEC system with other systems and optimizing the parameters can be employed. One of the ways to improve the performance of the OTEC cycle is to combine it with solar energy systems and wind turbines (Chen & Huo, 2023).

Yi et al. (2022) conducted a thermodynamic analysis of an OTEC system integrated with an ejector absorption power cycle prior to expansion, using MATLAB and Aspen Plus software. The results showed that turbine output increased by 79.38% with the pre-expansion process; however, this enhancement came at the expense of reduced thermal efficiency (Yi et al., 2022). Keshavarzzadeh et al. (2019) conducted a thermodynamic analysis and optimization of a fuel cell and electrolysis-based energy system for the simultaneous production of electricity, hydrogen, and cooling. Using the NSGA-II genetic algorithm for multi-objective optimization, the results indicated a total cost rate of $0.58 per second and an exergy efficiency of 80% (Keshavarzzadeh & Ahmadi, 2019). Zhou and Cao (2022) presented various plans to enhance the energy performance of a building located on the coast of Hong Kong, utilizing energy harnessed from tidal flow and photovoltaic systems (Zhou & Cao, 2022). Atiz et al. (2019) analyzed the performance of a renewable energy system featuring a 300-square-meter solar collector with evacuated tubes, designed to absorb solar radiation and produce both hydrogen and electricity. Their results showed exergy and thermal efficiencies of 18.21% and 5.92%, respectively (Atiz et al., 2019).

Islam et al. (2022) investigated suitable locations for the development of wind and solar energy in the northern regions of Queensland and South Australia. Their findings indicate that the potential capacity for wind and solar energy is 421.12 GW and 5956.14 GW, respectively (Islam et al., 2022). A concentrated solar system with an integrated supercritical carbon dioxide system was investigated by Hu and Wang (2023). Based on the findings, the use of these systems has increased exergy and energy efficiency (Hu & Wang, 2023). Jamil et al. (2023) conducted a thermodynamic and economic analysis of a solar power plant. Their findings indicate that the excess energy fed into the grid amounted to 1,504.32 megawatt-hours, generating a profit of $300,864.87 (Jamil et al., 2023). Mao et al. (2023) conducted a numerical analysis of temperature distribution and heat transfer characteristics in cold-water pipes of an OTEC system, examining the effects of wall thickness and flow rate on outlet temperature. Their findings indicate that the temperature of the cold seawater increased continuously throughout the process (Mao et al., 2023). Wang et al. (2011) conducted a thermodynamic analysis of OTEC systems using different working fluids for low-grade heat conversion (Wang et al., 2011). Liu et al. (2004) performed a thermodynamic analysis of an OTEC system using various working fluids. Their findings indicate that energy efficiency depends on the critical temperature of the working fluid. Additionally, wet working fluids are unsuitable for Organic Rankine Cycle (ORC) systems due to hydrogen bonding effects (Liu et al., 2004). Gong et al. (2013) evaluated the performance of an OTEC system using various working fluids to ensure stable pump and turbine operation. Their findings indicate that the R125 working fluid delivers the best performance (Gong et al., 2013). Yoon et al. (2014) studied the operation of an OTEC system using different working fluids to improve efficiency. Their findings show that ammonia exhibits the highest thermal efficiency (Yoon et al., 2014). An OTEC system using various working fluids—including R152a, R134a, R717, R227ea, R600a, and R601—was investigated for multi-objective optimization of levelized cost of energy (LCOE) and exergy efficiency. Among these fluids, R717 and R601 demonstrated the best overall performance (Wang et al., 2018). Hall et al. (2022) analyzed the advantages and disadvantages of OTEC systems. Their findings suggest that selecting the appropriate working fluid and making informed operational decisions can maximize the thermal energy extraction from the ocean,

thereby improving thermodynamic efficiency (Hall et al., 2022). This study integrates machine learning with single-objective and multi-objective optimization (NSGA-II) to assess the impact of various working fluids in hybrid OTEC systems, presenting a novel approach beyond prior thermodynamic-focused research. Working fluids are critical in determining energy conversion efficiency, influencing both power output and cycle performance. By comparing different fluids, the study aims to identify the most effective candidates for optimizing cycle efficiency and overall operational outcomes. Simulated data from the Caspian Sea were used, providing a contrast to the data employed by Hosseinzadeh et al., which were based on Bandar Abbas and Karkheh Dam (Hoseinzadeh et al., 2023). The cycle was evaluated using energy, exergy, and economic analyses. Energy analysis identifies work output and areas of energy loss, while exergy analysis assesses the quality of energy transformations within the system. Economic analysis, meanwhile, examines the cost-effectiveness of the cycle. Together, these analyses provide a comprehensive assessment of the system's efficiency and financial viability.

2. Systems description

Figure 1 presents schematic diagrams of the three proposed plans: Plan A (base OTEC cycle with thermoelectric integration), Plan B (OTEC cycle combined with a wind turbine), and Plan C (OTEC cycle with a condenser replacing the thermoelectric component). The figure details the seawater heating process, solar collector operation, turbine and pump configurations, and cooling mechanisms. For example, the schematic of Plan A (Figure 1) illustrates the process of pumping seawater into the system. To enhance heat production, seawater passes through a solar collector, increasing its temperature (point 7). The heated fluid then flows to the evaporator, where heat is transferred to the organic Rankine cycle. The cooled seawater (point 8) is returned to the ocean, completing a continuous loop. Within the cycle, the working fluid enters the turbine as saturated steam (point 1) to generate electricity. It subsequently passes through the thermoelectric generator (point 2), producing additional electricity. The resulting saturated liquid is then pumped from the thermoelectric generator (point 3), and the cycle repeats. Deep seawater is used to cool the thermoelectric generator (point 10).

The three energy production systems focus respectively on solar, wind, and ocean thermal energy, evaluated based on the potential of different plan locations. Plan A serves as the base cycle, while Plans B and C represent proposed hybrid configurations. Since solar energy availability varies by time of day, season, and location, it is assessed on an hourly basis in all systems. Additionally, the number of solar collectors for each cycle is determined according to local climate conditions. These systems are generally designed for coastal areas with significant ocean thermal energy potential, characterized by a notable temperature difference between the ocean surface and deep water. For wind energy integration, a 1 MW wind turbine is incorporated into the system.

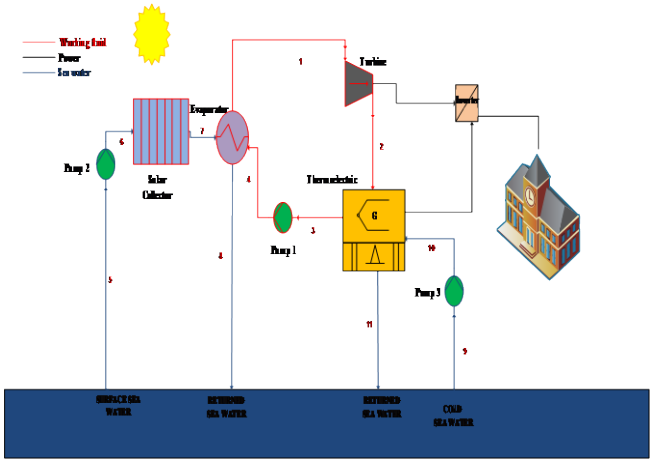

Basic: Plan A

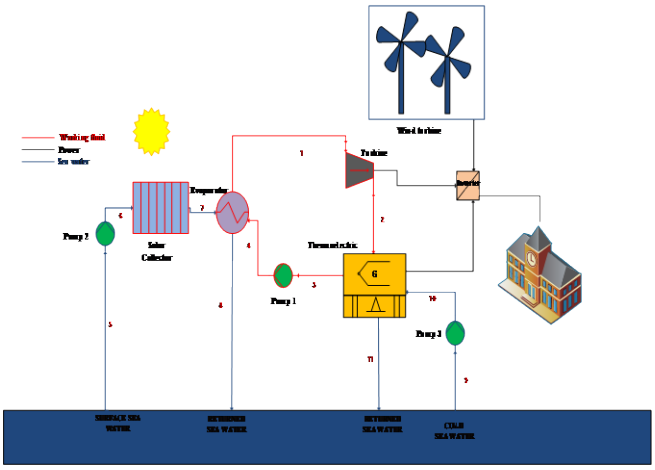

Plan B

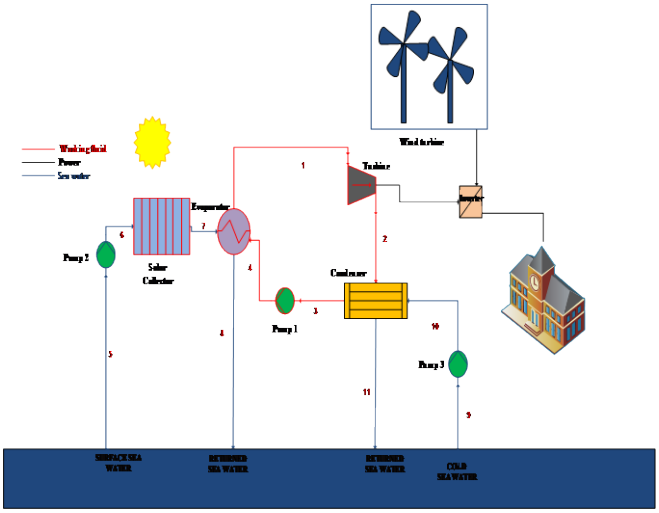

Plan C

Figure 1. Schematic of the OTEC for three plans.

3. Energy, exergy, and economic analysis

3.1. Study energy

In thermodynamic modeling, two fundamental laws are applied: the law of conservation of mass and the law of conservation of energy, as expressed in relations (1) and (2). According to the mass conservation principle, the total mass entering a system must equal the total mass exiting it, ensuring no mass is lost or created during the process. Similarly, the law of conservation of energy states that the energy received by the system must equal the energy leaving the system, meaning energy can neither be created nor destroyed, only transformed or transferred (Hoseinzadeh et al., 2023). The following assumptions are considered for system analysis (Hoseinzadeh et al., 2023).

- System operates under stable conditions.
- Turbines and pumps are isentropic.
- The pressure drop along the pipelines is neglected since its impact on the overall cycle performance is minimal (Mehrpooya et al., 2021).
- The inlet to the turbine is saturated steam and the inlet to the pump is saturated liquid.
- Changes in potential and kinetic energy are neglected in this kinetic and potential energy analysis (Delpisheh et al., 2021).

$$\sum_{in} \dot{m}_{in} h_{in} - \sum_{out} \dot{m}_{out} h_{out} - \dot{W} + \dot{Q} = 0 \quad (1)$$

$$\sum_{i} (\dot{m}_{in} - \dot{m}_{out}) = 0 \quad (2)$$

3.1.1. Solar unit analysis

The energy produced in the solar collector is calculated from Equations (3) and (4) by evaluating the fluid flow rate and inlet and outlet temperatures (Assareh et al., 2022; Delpisheh et al., 2021).

$$\dot{Q}_U = A_C . F_R [S - U_L (T_8 - T_a)] \quad (3)$$

$$F_R = \frac{\dot{m}_{WF}}{A_C U_L} \left[1 - \exp\left(-\frac{A_C U_L F'}{\dot{m}_{WF} C_P}\right)\right] \quad (4)$$

In the above relationships, F_R is the heat loss coefficient, F' The coefficient of efficiency of the collector and its value is 0.841, S is the flux of solar radiation, U_L is the overall heat loss coefficient and its value $0.8 \frac{W}{m^{2\circ}C}$, and T_a is the ambient temperature.

The output temperature from the solar collector is calculated using Equation (5).

$$\dot{Q}_U = \dot{m}_{WF} . C_P (T_9 - T_8) \quad (5)$$

3.1.2. Thermoelectric analysis

To analyze the thermoelectric output and the electricity generated by the thermoelectric system, the following equations are employed. Specifically, Equation (6) defines the energy input to the system as the sum of the energy outputs and the electrical power generated by the thermoelectric unit (Akrami et al., 2018; Wang & Hung, 2010):

$$\dot{W}_{TEG} = \dot{m}_3 (h_3 - h_2) \quad (6)$$

In this equation, the thermoelectric power output ($\dot{W}_{TEG}$) is calculated as the difference between the input and output thermal energies. To calculate the thermoelectric efficiency, Equation (7) is used, which gives the system efficiency as the product of the Carnot efficiency (η_{Carnot}) and a correction factor:

$$h_{TEG} = \eta_{Carnot} \times \left(\left(\sqrt{1 + ZT_M}\right) - 1\right) + \frac{T_L}{\left(\sqrt{1 + ZT_M}\right) + \left(\frac{T_L}{T_H}\right)} \quad (7)$$

In this equation, ZT_M is the figure of merit of the material, which is considered constant with a value of 0.8. The Carnot efficiency is calculated using Equation (8):

$$\eta_{Carnot} = 1 - \left(\frac{T_L}{T_H}\right) \quad (8)$$

Here, T_H and T_L represent the cold and hot source temperatures, respectively. In addition, the heat entering the system is calculated using Equation (9) based on the enthalpy change:

$$Q_{Elegant} = \dot{m}_6 (h_6 - h_7) \quad (9)$$

In this equation, the change in enthalpy between two different states of the system determines the heat entering the system. To calculate T_H and T_L, Equations (10) and (11) are used as follows:

$$T_H = 0.5(T_2 + T_3) \quad (10)$$

$$T_L = 0.5(T_{10} + T_{11}) \quad (11)$$

These equations are essential for analyzing and optimizing the performance of thermoelectric systems. The system's efficiency is highly influenced by the temperature gradient, the thermoelectric material properties, and the effectiveness of heat transfer within the system.

3.1.3. Wind turbine analysis

To calculate the performance of the wind turbine, the area swept by the turbine blades is first determined using Equation (12) (Hoseinzadeh et al., 2023):

$$A_{wt} = D^2 \frac{\pi}{4} \quad (12)$$

In this equation, A_{wt} represents the area swept by the wind turbine blades, and D is the diameter of the turbine.

Next, the power generated by the wind turbine is calculated using Equation (13):

$$W_{wt} = \frac{1}{2} \eta_{wt} \rho_{air} A_{wt} \eta_{ecoefficiency} V_{avg.wind}{}^3 \frac{4}{1000} \quad (13)$$

In this equation, W_{wt} represents the power generated by the wind turbine. Here, η_{wt} is the efficiency of the turbine, ρ_{air} is the air density, A_{wt} is the area swept by the blades, η_{eco} is the system efficiency, and $V_{avg.wind}$ is the average wind speed. The factor 4/1000 is used to convert the result into kW.

The overall energy inlet rate is obtained from Equation (14).

$$Input = \frac{1}{2} \rho_{air} A_{wt} \eta_{ecoefficiency} V_{avg.wind}{}^3 \frac{4}{1000} \quad (14)$$

These equations (13) and (14) are generally used to estimate the power output of the wind turbine based on its physical dimensions, wind conditions, and system efficiencies.

The governing equations for different cycle equipment are shown in Table 1.

Table 1. Relationships used for energy analysis of the suggested cycle (Dezhdar et al., 2023; Hoseinzadeh et al.).

Equipment	Relation
Generator	$\dot{W}_G = \eta_G.(\dot{W}_{Turbine})$
Turbine OFC	$\dot{W}_{Turbine} = \dot{m}_1.(h_1 - h_2)$
Condenser	$\dot{Q}_{Condenser} = \dot{m}_2.(h_2 - h_3)$
Evaporator	$\dot{Q}_{Evaporator} = \dot{m}_4.(h_1 - h_4)$
Pump working fluid	$\dot{W}_{Pump\ 1} = \dot{m}_3.(h_4 - h_3)$
Warm water pump	$\dot{W}_{Pump\ 2} = \dot{m}_5.(h_6 - h_5)$
Cold water pump	$\dot{W}_{Pump\ 3} = \dot{m}_9.(h_{10} - h_9)$

3.1.4. Wind turbine analysis

Energy efficiency is considered a crucial metric for assessing the performance of the system, as it is derived from Equations (15) and (16).

$$\dot{W}_{net} = \dot{W}_G - \dot{W}_{Pump\ 1} - \dot{W}_{Pump\ 2} - \dot{W}_{Pump\ 3} + \dot{W}_{Wind\ turbine} + \dot{W}_{TEG} \quad (15)$$

$$\eta_{en} = \frac{\dot{W}_{net}}{\dot{Q}_{Eva}} \quad (16)$$

3.2. Exergy study

Exergy efficiency quantifies how effectively a system converts available energy into useful work, taking into account both the quantity and quality of energy, as shown in relations (17) to (20). It offers valuable insight into energy utilization by assessing losses and irreversibilities within the system. In this study, the following equations are applied to conduct the exergy analysis (Ahmadi et al., 2013). The relationships used are shown in Table 2 (Ahmadi et al., 2013; Assareh et al., 2021; Dezhdar et al., 2023; Hoseinzadeh et al., 2023; Shahin et al., 2023; Sinama et al., 2015).

$$\dot{E}_X^Q + \sum_i \dot{m}_i ex_i = \sum_e \dot{m}_e ex_e + \dot{E}_X^W + \dot{I} \quad (17)$$

$$\dot{E}_X^Q = (1 - \frac{T_0}{T_i})\dot{Q}_i \quad (18)$$

$$ex = ex_{ph} + ex_{ch} \quad (19)$$

$$ex_{ph} = (h - h_0) - T_0(S - S_0) \quad (20)$$

3.2.1. System exergy efficiency

Exergy efficiency is considered a crucial metric for assessing the performance of the system, as it is derived from Equation (21):

$$\eta_{ex} = \frac{\dot{W}_{net}}{E_9 + E_{Sun} + Input} \quad (21)$$

3.3. Economic study

Economic analysis assesses the cost-efficiency of various systems by evaluating both equipment and operational expenses, providing insights into the financial feasibility and economic impact of each cycle. To estimate the cost of individual components and the total system cost rate, specific cost functions are applied to each element. The cost rate is determined using economic parameters such as the capital recovery factor and interest rate, enabling a more precise evaluation of the system's overall economic performance. The cost rate for each component is defined by Equation (22) (Houshfar, 2020):

$$\dot{Z}_K = \frac{\emptyset_K \times Z_K \times CRF}{hour} \quad (22)$$

In this equation, $\dot{Z}_K$ represents the cost rate and ϕ_K is the repair and maintenance factor, which is set to 1.06. *hour* is the system's operating hours, which is 7446 hours. The Capital Recovery Factor (CRF) is calculated using the formula in Equation (23) (Habibollahzade et al., 2018):

$$CRF = \frac{i \times (1+i)^n}{(1+i)^n - 1} \quad (23)$$

Here, i and n refer to the profit rate and the plant's operational cycle (in years), which are 0.1 and 20, respectively. Table 3 illustrates the cost for each element, and the required auxiliary equations are also provided.

Table 2. Equations used for modified cycle exergy analysis (Ahmadi et al., 2013; Assareh et al., 2021; Dezhdar et al., 2023; Hoseinzadeh et al., 2023; Shahin et al., 2023; Sinama et al., 2015).

Subsystems	Equations	Exergy efficiency
Wind turbine	$\dot{I}_{wt} = \left(\frac{W_{wt}}{C_{p,wt}}\right)$	$\psi_{wt} = \left(\frac{\frac{1}{2}\rho_{air}A_{wt}V_{avg.wind}^{\ 3}}{Input}\right)$
Turbine	$\dot{I}_{Turbine} = (E_1 - E_2) - \dot{W}_{Turbine}$	$\psi_{Turbine} = \left(\frac{\dot{W}_{Turbine}}{E_1 - E_2}\right)$
Evaporator	$\dot{I}_{Eva} = (E_7 + E_4) - (E_1 + E_8)$	$\psi_{Eva} = \left(\frac{E_1 - E_4}{E_7 - E_8}\right)$
Warm water Pump	$\dot{I}_{Pump\ 2} = (E_5 + \dot{W}_{Pump\ 2}) - (E_6)$	$\psi_{Pump\ 2} = \left(\frac{E_6 - E_5}{\dot{W}_{Pump\ 2}}\right)$
Cold water Pump	$\dot{I}_{Pump\ 3} = (E_9 + \dot{W}_{Pump\ 3}) - (E_{10})$	$\psi_{Pump\ 3} = \left(\frac{E_{10} - E_9}{\dot{W}_{Pump\ 3}}\right)$
Pump working fluid	$\dot{I}_{Pump\ 1} = (E_6 - E_7) + \dot{W}_{Pump\ 1}$	$\psi_{Pump\ 1} = \left(\frac{E_4 - E_3}{\dot{W}_{Pump\ 1}}\right)$
Condenser	$\dot{I}_{Con} = (E_2 + E_{10}) - (E_3 + E_{11})$	$\psi_{Con} = \left(\frac{E_2 - E_3}{E_{11} - E_{10}}\right)$
Solar collector	$\dot{I}_{collector} = E_{Sun} + E_6 - E_7$	$\psi_{Collector} = \left(\frac{E_6}{E_7 + E_{Sun}}\right)$
Thermoelectric	$\dot{I}_{TEG} = (E_{10} + E_2) - (E_3 - E_{11}) - \dot{W}_{TEG}$	$\psi_{Con} = \left(\frac{\dot{W}_{TEG}}{E_4 - E_6}\right)$
Generator	$\dot{I}_G = (1 - \eta_G)(\dot{W}_{Turbine})$	
Exergy output from the cycle	$\dot{I}_{loss} = E_8 + E_{11}$	

Table 3. Equipment cost (Dezhdar et al., 2023; Hoseinzadeh et al.; Tsatsaronis & Morosuk, 2008).

Equation description/element	Equation
Total cost	$Z_{Total} = Z_{Evaporator} + Z_{Pump} + Z_{Turbine} + Z_{Solar\ Collector} + Z_{Wind\ Turbine} + Z_{Condenser} + Z_{TEG}$
Turbine	$Z_{Turbine} = 4750 \times (\dot{W}_{Turbine}^{0.41}) + 60 \times (\dot{W}_{Turbine}^{0.95})$
Evaporator	$Z_{Eva} = 276 \times (A_{Evap}^{0.88})$
Condenser	$Z_{Con} = 1500 \times (\dot{W}_{Condenser}^{0.8})$
Pump	$Z_{Pump} = 3500 \times (\dot{W}_{Pump}^{0.41})$
Solar Collector	$Z_{Solar\ collector} = 235 \times (A_p)$
Wind turbine	$Z_{Wind\ turbine} = 5000 \times (\dot{W}_{Wind\ turbine})$
Thermoelectric	$Z_{TEG} = 1500 \times (\dot{W_{TEG}})$

3.4. System parameters used in the simulation

The annual variations in seawater salinity and the temperature profile relative to depth—both essential for the thermodynamic analysis of the cycle's components—are illustrated in Figures 2 and 3 (Hoseinzadeh et al., 2024). The parameters used in the simulation of different parts of the cycle are shown in Table 4 (Hoseinzadeh et al., 2023).

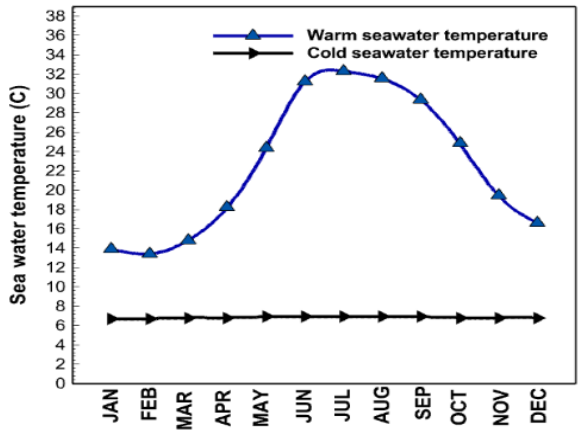

Figure 2. Curve of monthly temperature changes of the surface waters and 200 meters depth of the sea.

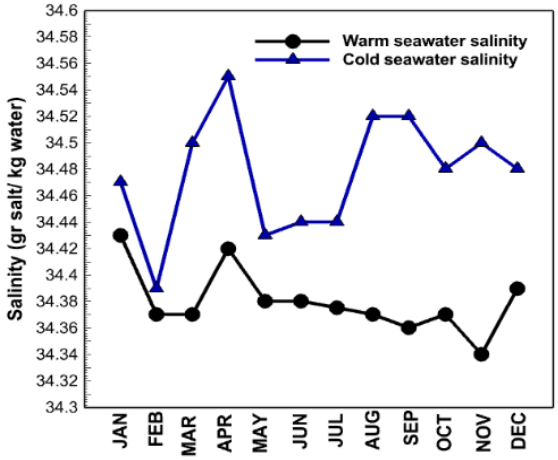

Figure 3. Curve of monthly salinity changes of surface waters and 200 meters depth of the sea.

In this system, T_0 and P_0 represent the ambient temperature and pressure, respectively. P_5, P_6, P_9, and P_{10} represent the inlet pressure to the hot water pump, the outlet pressure from the hot water pump, the inlet pressure to the cold water pump, and the outlet pressure from the cold water pump, respectively. F_R, I, T_{Sun}, and U_L represent the collector efficiency factor, the solar irradiance in the area, the temperature of the sun, and the heat loss factor of the collector, respectively. T_3 indicates the temperature of the working fluid entering the pump. PP_{Evap} represents the evaporation temperature at the pinch point in the evaporator. The system's efficiencies include the pump efficiency η_{Pump} and the turbine efficiency $\eta_{Turbine}$. The average wind speed V_{Wt} is also considered. Finally, the wind turbine efficiency $\eta_{Windturbine}$ and the wind turbine blade diameter $D_{Windturbine}$ are specified.

Table 4. Input data for simulating the suggested cycle (Dezhdar et al., 2023; Hoseinzadeh et al., 2023).

Designparameter	value	unit
T_0	25	˚C
P_0	101.325	kPa
P_5	101.325	kPa
P_6	150	kPa
$\dot{m}_5$	30	kg/s
F_R	0.914	m
I	800	W.m^{-2}
T_{Sun}	5770	k
U_L	3.82	m
T_3	15˚	˚C
P_9	150	kPa
P_{10}	600	kPa
PP_{Eva}	10	˚C
η_{Con}	0.9	
η_{Pump}	0.85	
$\eta_{Turbine}$	0.8	
V_{Wt}	5.5	m/s
$\eta_{Wind\ turbine}$	0.9	
$D_{Wind\ turbine}$	34	m

4. Simulation results

4.1. Validation

The thermoelectric subsystem was chosen for validation due to its critical role in determining overall cycle efficiency. Its performance was benchmarked against the work of Habibollahzadeh et al. (Habibollahzade et al., 2018), showing less than 1% deviation (Figure 4), which confirms the model's accuracy. Additionally, comparisons with the work of Hoseinzadeh et al. for similar hybrid OTEC systems have shown consistency, with deviations under 1.5% in Table 5 (Hoseinzadeh et al., 2023). The consistency across multiple

validation points confirms the robustness and accuracy of the developed model.

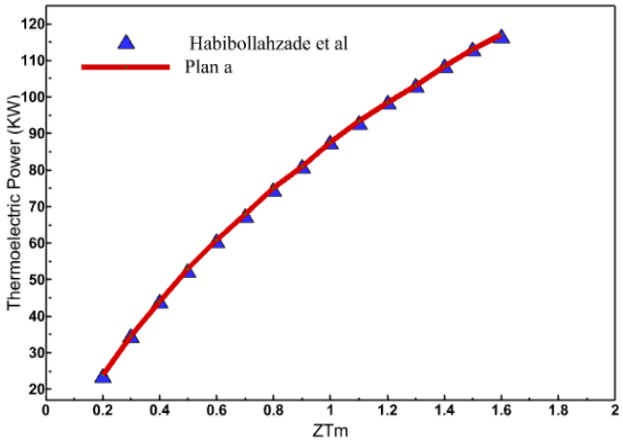

Figure 4. Comparison of thermoelectric results with the findings of Habibollahzadeh et al. (Habibollahzade et al., 2018).

Table 5: Validation of cycle results with research by Hoseinzadeh et al. (Hoseinzadeh et al., 2023)

Variable	Present	Hoseinzadeh et al.	Difference (%)
Exergy efficiency (%)	6.50	6.56	0.91
ORC power (kW)	249	247	0.80
Out net power (kW)	242	240	0.83
Thermoelectric power (kW)	17.7	17.5	1.14
Cost rate ($/h)	53.9	53.5	0.74

4.2. Production power

Figure 5 provides a compelling demonstration of the advantages of integrating multiple renewable energy technologies. By analyzing three distinct power generation schemes, the study highlights the superior performance of a hybrid system that combines thermoelectric technology with wind turbines. Plan B, which incorporates both thermoelectric and wind turbine systems, achieves the highest power output at 433.5 kW, outperforming Plan A (314.35 kW, thermoelectric only) and Plan C (297.85 kW, wind turbine only). This substantial increase underscores the synergistic benefits of a hybrid approach:

- **Complementary Resource Utilization**: Thermoelectric systems and wind turbines harness different forms of energy—thermal gradients and kinetic wind energy, respectively. Their integration enables the system to exploit a broader spectrum of renewable resources, thereby maximizing power generation potential.
- **Enhanced Reliability**: Utilizing two independent energy sources increases system resilience. If one component underperforms due to environmental conditions, the other can compensate, resulting in a more stable and reliable energy output.
- **Improved Efficiency**: The hybrid configuration enables better overall efficiency compared to standalone technologies. This improvement arises from optimized heat transfer, refined turbine design, and the capacity to tailor each subsystem for peak performance within the integrated system.

The results shown in Figure 5 strongly support the adoption of hybrid renewable energy systems. Compared to single-technology solutions, hybrid systems offer several distinct benefits:

- **Higher Energy Output**: By combining technologies, hybrid systems are capable of producing significantly greater power to meet increasing energy demands.
- **Improved Reliability**: The dual-source configuration ensures a more stable and consistent energy supply, reducing dependence on fossil fuels.
- **Cost-Effectiveness**: Leveraging the strengths of multiple technologies can lead to lower overall energy production costs by improving system efficiency and reducing operational vulnerabilities.

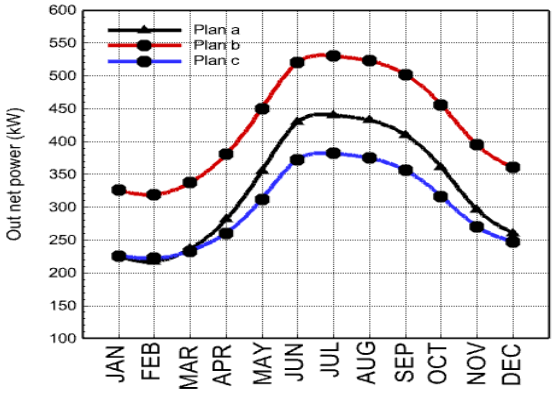

Figure 5. Investigation of net useful work for three plans A, B, and C.

4.3. Energy and exergy productivity

Plan B achieves an average thermal efficiency of 11%, outperforming Plan C at 9.98% and Plan A at 5.81%. This result indicates that Plan B exhibits the highest thermal efficiency, primarily due to the synergistic integration of turbine and thermoelectric power systems. Although Plan C demonstrates better performance than Plan A, it does not reach the efficiency level of Plan B. The thermal efficiency analysis presented in Figure 6 underscores the significant advantages of hybrid systems that combine thermoelectric and wind energy technologies. Plan B's superior performance highlights the potential of such hybrid configurations to enhance not only efficiency but also the reliability and sustainability of renewable energy systems. Continued research and optimization of these integrated technologies can contribute to a cleaner, more resilient energy infrastructure.

Figure 7 presents the monthly average exergy efficiency of the three proposed cycles. Plan B again demonstrates the highest exergy efficiency, confirming the effectiveness of combining wind turbine technology with a thermoelectric system. This hybrid approach optimizes both energy conversion and resource utilization, resulting in enhanced overall system performance. Plan A, with an average exergy efficiency of 6.52%, shows moderate effectiveness, as it relies solely on thermoelectric power. Plan C, which depends exclusively on wind energy, records the lowest exergy efficiency at 6.10%, indicating less effective energy conversion compared to the other plans. These findings suggest that technological integration, as implemented in Plan B, significantly improves exergy efficiency by enhancing energy management and conversion processes.

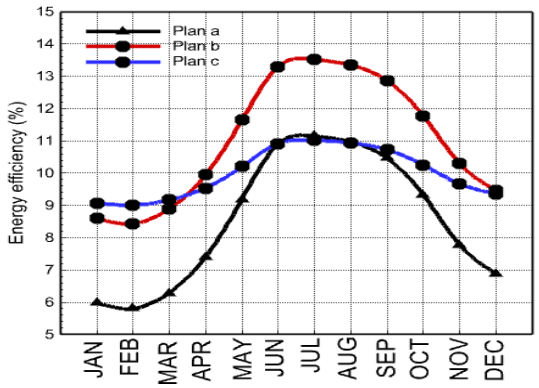

Figure 6. Comparing the energy productivity for three plans A, B and C.

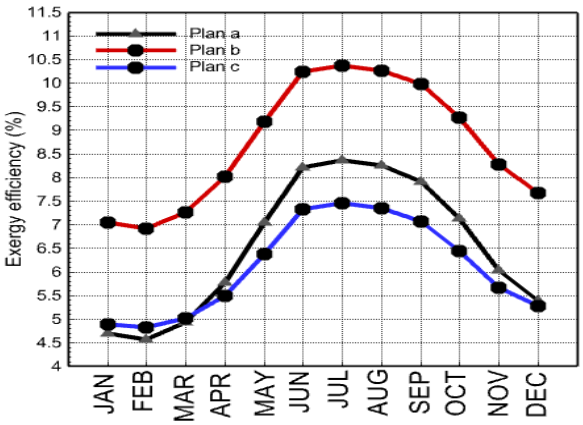

Figure 7. Comparing the exergy productivity for three plans A, B and C.

4.4. Total exergy destruction

Figure 8 illustrates the total exergy destruction of the three proposed plans throughout the year. Notably, all three plans exhibit peak exergy destruction during the summer months (June, July, and August), primarily due to elevated surface water temperatures that exacerbate thermal irreversibilities and thereby increase exergy losses. Among the plans, Plan A demonstrates the highest exergy destruction across all months, highlighting the limited performance and higher inefficiencies of a standalone thermoelectric system.

In contrast, Plan B shows reduced exergy destruction, attributable to the integration of a wind turbine, which enhances power generation and overall system efficiency by diversifying energy inputs. Plan C, which replaces the thermoelectric component with a condenser, consistently records the lowest exergy destruction, indicating more effective thermal energy management and reduced irreversibility within the cycle.

Table 6 presents the exergy efficiencies of key system components. In Plan A, the exergy efficiency of the thermoelectric unit and solar collector is relatively low, at 9.23% and 6.27%, respectively, while the turbine and pumps demonstrate comparatively higher efficiencies. Plan B, benefiting from the addition of the wind turbine, achieves a turbine efficiency of 53.1%; however, the thermoelectric and solar collector efficiencies remain limited. Plan C demonstrates a notable improvement with an 85% exergy efficiency for the condenser, underscoring its effectiveness in reducing losses. Overall, the incorporation of either a wind turbine (Plan B) or a condenser (Plan C) leads to improved exergy efficiency when compared to the base system in Plan A.

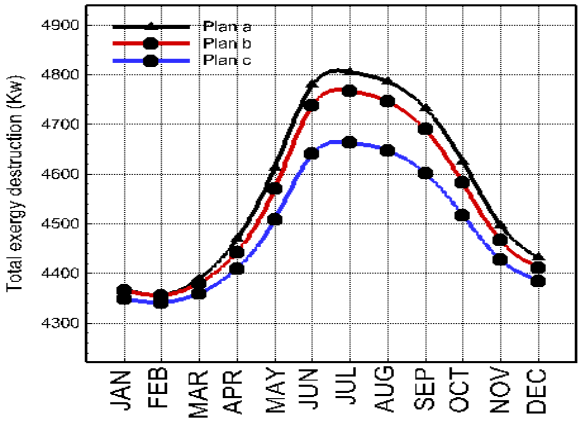

Figure 8. Comparison of exergy destruction for three plans A, B, and C.

Table 6. Exergy efficiency of equipment.

	Cycle		
Equipment (%)	**Plan A**	**Plan B**	**Plan C**
Evaporator	72.83	73.31	82.22
Pump 1	84.38	84.39	84.39
Pump 2	99	99.1	99.23
Pump 3	100	100	100
Solar collector	9.22	8.44	8.44
TEG	6.27	9.422	-
Turbine	80.23	80.19	80.19
Wind turbine	-	53.1	53.1
Condenser	-	0	85

4.5. Economic Analysis

Figure 9 presents the average equipment cost rates for the three cycles: Plan A, Plan B, and Plan C. Plan B incurs the highest average cost at $60.81 per hour, reflecting the additional investment needed to integrate both thermoelectric technology and a wind turbine. Plan A, relying solely on the thermoelectric system, has the lowest average cost of $47.37 per hour, making it the most economical option. Plan C falls in between, with an average cost of $58.28 per hour—more affordable than Plan B but costlier than Plan A. Although Plan B delivers superior performance, this comes at a higher expense, whereas Plan A offers a more budget-friendly alternative.

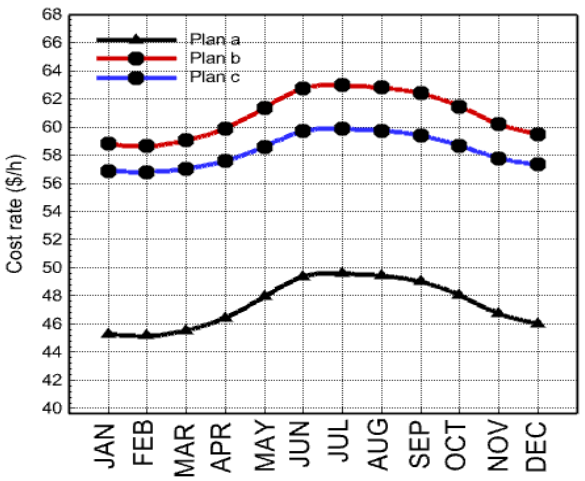

Figure 9. Comparison of the cost rate production for the three plans A, B, and C.

5. Analysis of working fluid

The independent variables in this study are the type of working fluid (R227ea, R152a, R125, R134a, R1234yf, R161, and Iso-butane), the system design (Plans B and C), and the monthly temperatures across different seasons. The dependent variables include power output, thermal efficiency, exergy efficiency, total equipment exergy destruction, and total equipment cost rate. A monthly analysis was performed to evaluate how seasonal variations impact system performance.

5.1. The effect of the working fluid on the productive work of the cycle

Figure 10(a) illustrates the impact of different working fluids on the useful power output of the cycle. Among the fluids tested, R227ea achieves the highest power output, indicating its superior effectiveness in energy conversion. R1234yf and Iso-butane also perform well, though slightly below R227ea. Conversely, R125 produces the lowest power output, highlighting its relative inefficiency within this cycle. These results emphasize the critical role of working fluid selection in optimizing cycle performance, with R227ea and R1234yf standing out as the most effective for generating useful work, while R125 is less favorable.

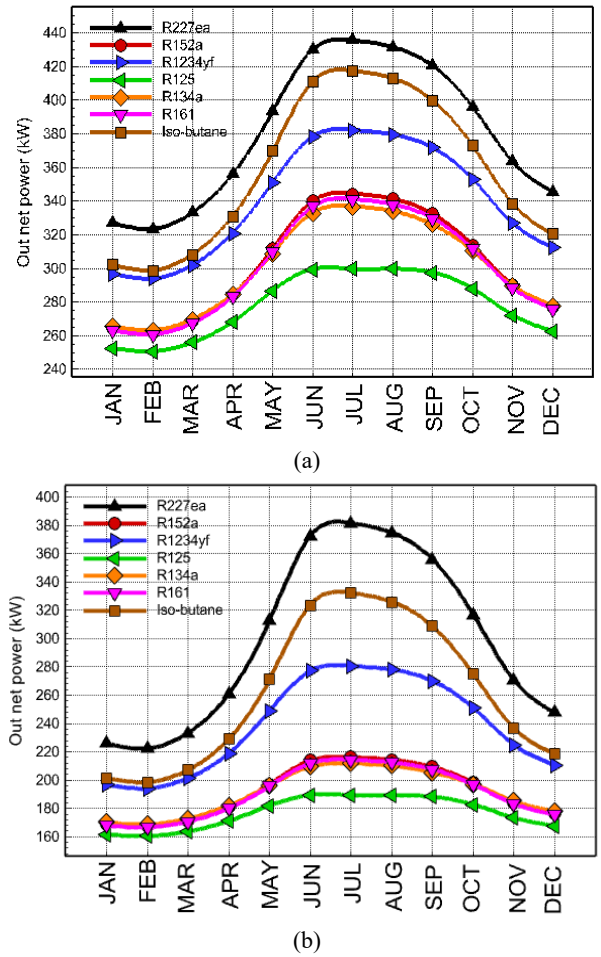

Figure 10. (a) The effect of different working fluids on the net useful work of plan B. **(b)** The effect of different working fluids on the net useful work of plan C.

Figure 10(b) focuses on the effect of working fluids on useful power output in Plan C. Here, the highest average output power is 380.6 kW for R227ea, while the lowest is 188.3 kW for R125. This again demonstrates R227ea's superior performance, whereas fluids like R125 and R134a show comparatively lower efficiency, reinforcing the importance of fluid choice on cycle efficiency.

When comparing the useful work output between Plan B and Plan C, Plan B—which integrates both thermoelectric technology and a wind turbine—consistently outperforms Plan C. Specifically, Plan B achieves its highest average power output of 433.5 kW with R227ea, while R125 produces the lowest at 297.7 kW. This suggests that the combined technologies in Plan B better harness the properties of each working fluid. In contrast, Plan C relies solely on the wind turbine, resulting in lower overall power outputs: 380.6 kW for R227ea and 188.3 kW for R125. This comparison highlights the advantage of integrating multiple renewable energy technologies, as exemplified by Plan B, to enhance energy conversion and maximize useful work output.

5.2. The effect of the working fluid on the thermal efficiency of the cycle

Figure 11(a) shows the average thermal efficiency of Plan B across various working fluids. R227ea achieves the highest thermal efficiency at 19.2%, closely followed by Iso-butane at 18.38%. R1234yf reaches 16.82%, while R125 records the lowest thermal efficiency at 13.35%. These results demonstrate the significant influence of working fluid choice on thermal performance in Plan B. Notably, R227ea and Iso-butane stand out as the most effective fluids for boosting thermal efficiency, underlining the importance of selecting the optimal fluid to improve cycle performance.

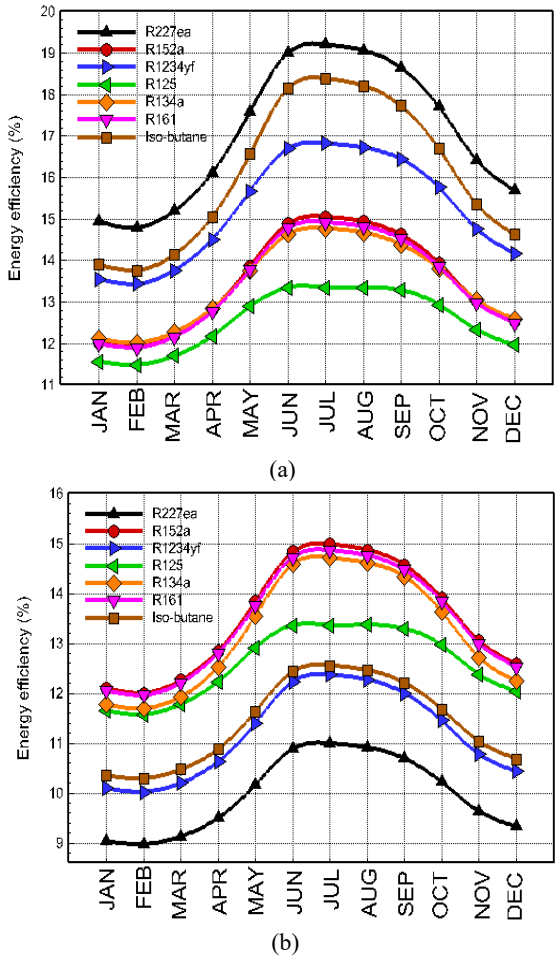

Figure 11. (a) The effect of different working fluids on the energy efficiency of plan B. **(b)** The effect of different working fluids on the energy efficiency of plan C.

Figure 11(b) presents the average thermal efficiency for Plan C with different working fluids. Here, R152a leads with a thermal efficiency of 14.98%, followed by R161 at 13.86% and R134a at 13.71%. Iso-butane and R1234yf show efficiencies of 12.55% and 12.37%, respectively, while R227ea ranks lowest at 10.99%. These findings confirm that fluid selection plays a key role in the thermal efficiency of Plan C, with R152a and R161 delivering the best performance.

Comparing the two plans, Plan B—which integrates thermoelectric technology and a wind turbine—achieves significantly higher thermal efficiencies across the tested fluids. For example, R227ea reaches 19.2% in Plan B but only 10.99% in Plan C. Similarly, R125 has the lowest efficiency in Plan B at 13.35%. The differences are likely due to variations in system design and operating conditions.

The lower efficiencies observed in Plan C, relative to Plan B, highlight the performance impact of excluding the thermoelectric system. Overall, this comparison underscores that Plan B's advanced integration of technologies leads to superior thermal efficiency, emphasizing the importance of incorporating such features to optimize thermodynamic cycle performance.

5.3. The effect of the working fluid on the exergy efficiency of the cycle

Figure 12(a) shows the average exergy efficiency for Plan B using different working fluids. Among them, R125 has the lowest exergy efficiency at 5.82%. In contrast, R227ea delivers the best exergy performance, demonstrating superior ability to convert available energy into useful work. The differences between fluids clearly illustrate how critical fluid selection is for exergy efficiency, with fluids like R227ea and Iso-butane outperforming others.

Figure 12(b) presents the average exergy efficiency for Plan C across the same set of working fluids. Here, R227ea again leads with the highest exergy efficiency at 7.44%, followed closely by Iso-butane at 7.15%. In comparison, R152a and R125 show notably lower efficiencies of 4.20% and 3.68%, respectively. These results confirm that R227ea and Iso-butane offer superior exergy performance, while the much lower efficiencies of fluids like R125 emphasize the importance of choosing the right working fluid to maximize exergy efficiency in the cycle.

5.4. The effect of the working fluid on the exergy destruction of the entire cycle equipment

Figure 13(a) displays the average exergy destruction for different working fluids in Plan B. Among these, R125 exhibits the highest exergy destruction, while Iso-butane shows the lowest. Although the differences in exergy destruction across fluids are relatively small, choosing a working fluid with lower exergy destruction can improve the overall performance and efficiency of Plan B.

Figure 13(b) illustrates the average exergy destruction for various working fluids in Plan C. R227ea has the lowest exergy destruction at 4663.2 kW, indicating the most efficient energy utilization among the tested fluids. In contrast, R125 shows the highest exergy destruction compared to R134a and R161. This analysis highlights R227ea as the most effective fluid for minimizing exergy destruction, thereby delivering better overall performance.

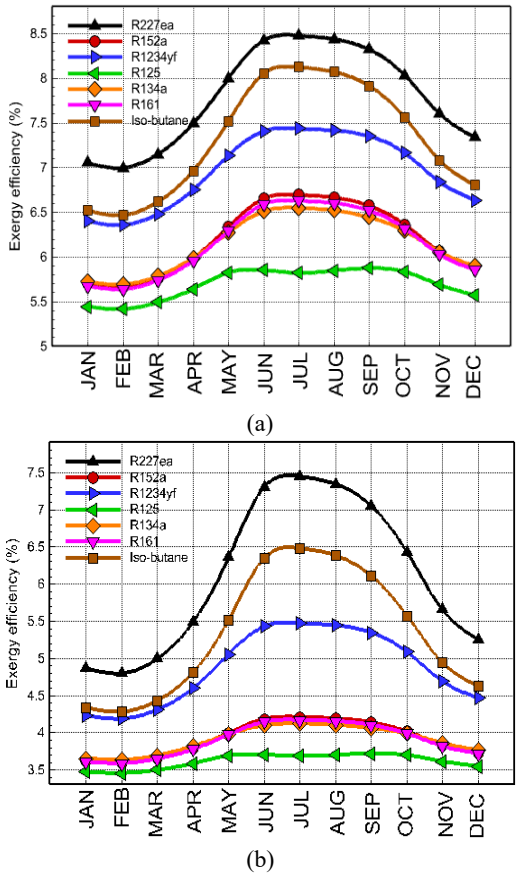

Figure 12. (a) The effect of different working fluids on the exergy efficiency of plan B. **(b)** The effect of different working fluids on the exergy efficiency of plan C.

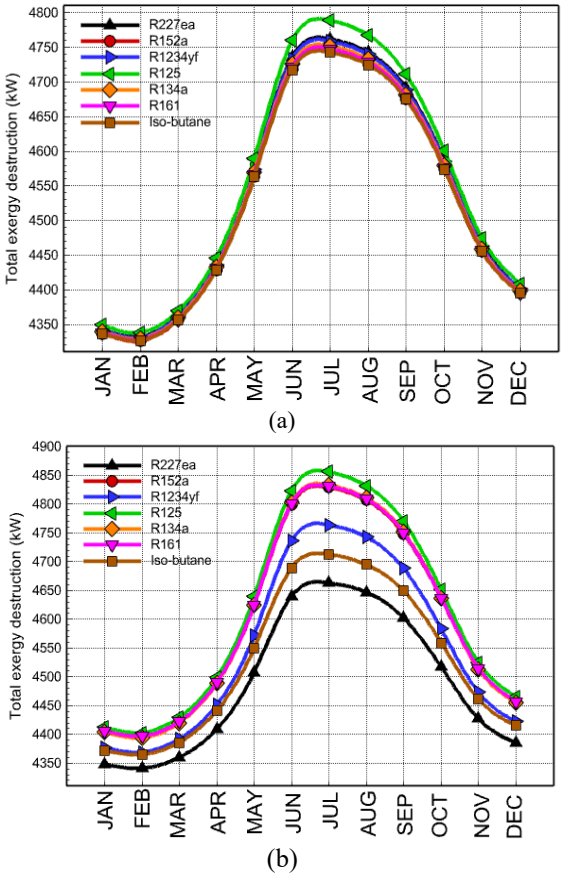

Figure 13. (a) The effect of different working fluids on the destruction of the total exergy of Plan B. **(b)** The effect of different working fluids on the destruction of the total exergy of Plan C.

When comparing the average exergy destruction between Plan B and Plan C, Plan B demonstrates more consistent performance with minimal variation across different working fluids. R125 exhibits the highest exergy destruction in Plan B at 4795 kW. This stability reflects the effective integration of thermoelectric systems and wind turbines in Plan B. In contrast, Plan C shows greater variability in exergy destruction among fluids, with R125 again causing the highest value at 4856 kW. This indicates that Plan C's performance is more sensitive to the choice of working fluid. Overall, Plan B offers a more stable exergy destruction profile, while Plan C's exergy destruction varies considerably depending on the fluid used.

5.5. The effect of the working fluid on the total cost rate of the cycle equipment

Figure 14(a) shows the average monthly cost rate for different refrigerants in Plan B, revealing that R227ea is the most expensive refrigerant, while R125 is the least costly. Figure 14(b) presents the average monthly cost rate for various refrigerants in Plan C, illustrating how refrigerant choice impacts equipment performance and operating costs. R125 remains the most economical option at $56.55 per hour, whereas R227ea incurs the highest cost at $59.87 per hour. A comparison between Plan C and Plan B shows that Plan C generally has lower average monthly equipment costs. For instance, R227ea costs $59.87 per hour in Plan C, compared to $61.65 per hour in Plan B, making Plan C the more affordable option overall.

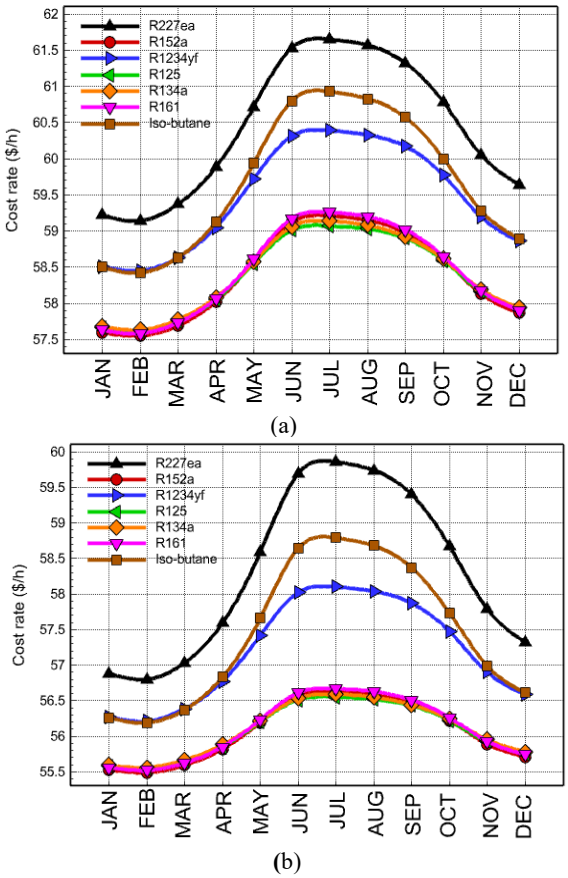

Figure 14. (a) The effect of types of working fluid on the cost rate of Plan B. **(b)** The effect of type of working fluid on the cost rate of Plan C.

The sensitivity analysis attributes R227ea's superior performance to its optimal thermodynamic properties, such as a high critical temperature (102.8°C) and favorable pressure characteristics, which improve the cycle's energy conversion efficiency. Moreover, R227ea's low global warming potential (GWP) enhances its environmental appeal. In contrast, R125 shows lower performance, primarily due to its reduced heat transfer efficiency and higher operating costs. The observed correlation between thermodynamic properties and performance indicates that fluids with higher latent heat and lower specific volume tend to achieve better cycle efficiency.

6. Optimization using NSGA-II based on EES data

A supervised machine learning model using Random Forest Regression (RFR) was developed in MATLAB to predict system performance. Input variables included turbine efficiency, solar radiation intensity, wind speed, and working fluid type, while output variables comprised output power, energy efficiency, and exergy efficiency. The dataset was split into 80% for training and 20% for testing. Hyperparameter tuning was conducted via Grid Search with cross-validation to prevent overfitting. The final model achieved a coefficient of determination (R^2) of 0.98 and a mean squared error (MSE) of 0.015, demonstrating high predictive accuracy. Both single-objective and multi-objective optimizations were performed to assess system performance. Multi-objective optimization aimed to maximize energy and exergy efficiencies while minimizing costs. The study focused on Plan B and Plan C cycles for the month of July, using R227ea as the working fluid. Initial data points were generated with Engineering Equation Solver (EES) and served as input for the NSGA-II (Non-Dominated Sorting Genetic Algorithm II) algorithm. The optimization process, outlined in the flowchart in Figure 15, involves several key steps: defining the objectives, generating initial data, evaluating system performance, and applying non-dominated sorting along with crowding distance to select and evolve solutions. This iterative process continues until convergence, ultimately producing a Pareto front that presents the optimal trade-offs between energy efficiency, exergy efficiency, and cost.

6.1. Single-Objective Optimization: Effect of Design Parameters

Table 7 shows the six key design variables used in the optimization process. These variables are investigated in both single-objective and multi-objective optimization:

- In single-objective optimization, these variables were optimized to find maximum energy efficiency or maximum exergy efficiency or minimum cost rate.
- In multi-objective optimization, three optimization criteria were considered simultaneously, including energy efficiency, exergy efficiency, and total system cost.

Table 8 shows the effect of simultaneous changes in turbine efficiency, collector area, solar radiation intensity, wind speed, turbine inlet pressure, and turbine inlet temperature on system performance. The results show that tuning these parameters has a significant effect on energy efficiency, exergy efficiency, and overall cost rate, which emphasizes the importance of a comprehensive approach to optimization.

6.2. Multi-Objective Optimization: Trade-Off Between Energy, Exergy, and Cost

Table 9 and Figure 16 present the Pareto fronts resulting from the multi-objective optimization of the Plan B and Plan C cycles. In such optimization, a single solution cannot simultaneously maximize all objectives. Instead, a set of non-

dominated solutions is generated, offering balanced trade-offs among energy efficiency, exergy efficiency, and cost. Figure 16 illustrates these trade-offs—for instance, improving energy efficiency often leads to increased cost, while minimizing cost may reduce exergy efficiency. This enables decision-makers to select the most suitable solution based on specific performance or economic priorities. The results indicate that, in Plan B, the energy efficiency, exergy efficiency, and cost rate are 9.51%, 0.95%, and 2.44%, respectively. In Plan C, the three-objective optimization yields improvements in energy efficiency and cost rate by 4.08% and 2.53%, respectively.

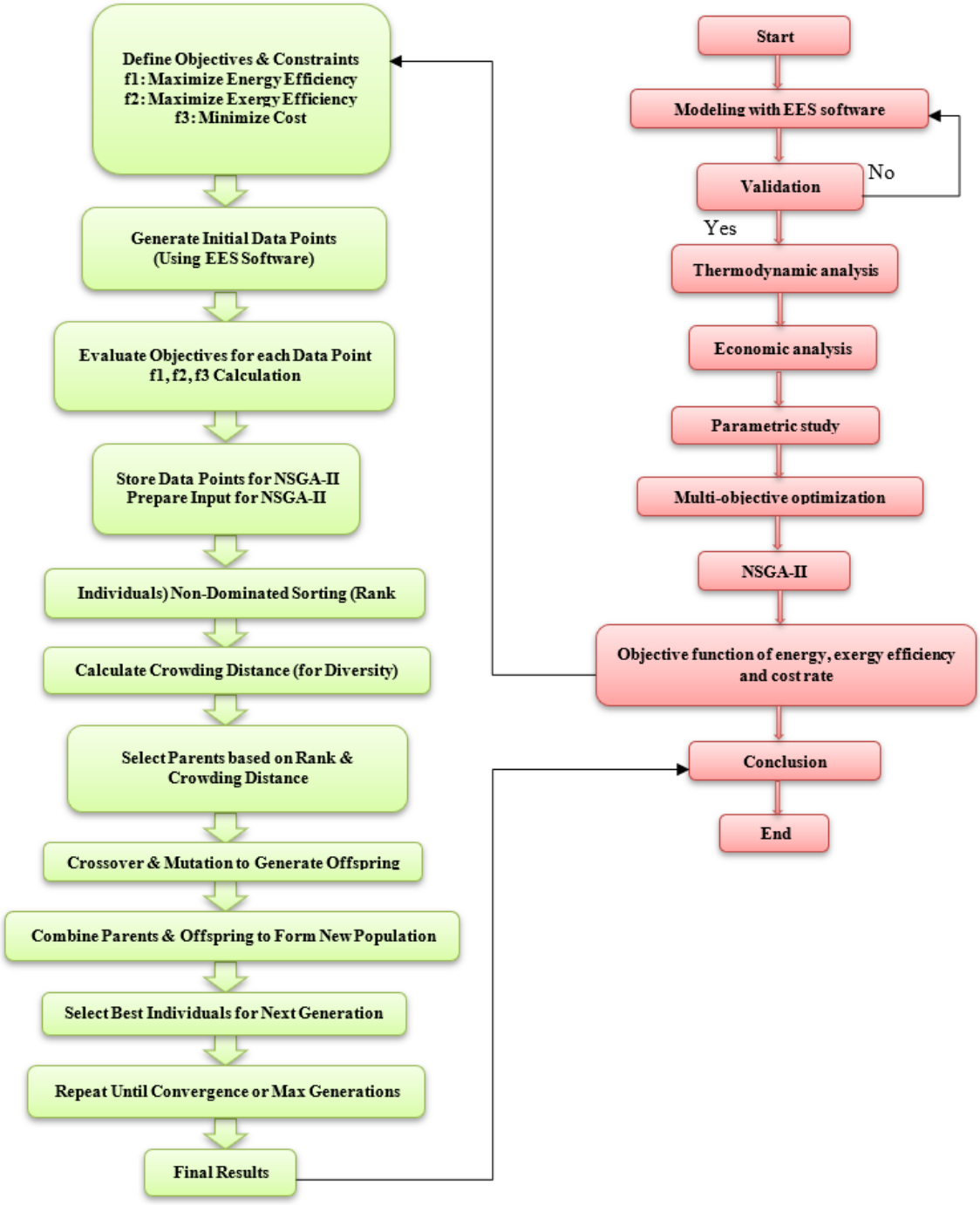

Figure 15. Flowchart of multi-objective optimization methodology

Table 7. Optimization variables and their range.

Name	Low level	High level
Collector area, $A_P(m^2)$	5000	15000
T_1(℃)	40	100
$P_1(kPa)$	400	1000
Solar radiation, I $(\frac{W}{m^2})$	200	2000
Average wind turbine speed, V_{wt} $(\frac{m}{s})$	2	10
Turbine efficiency, $\eta_{Turbine}$ (%)	0.2	1

Table 8. Multivariable and single-objective optimization results for plan B.

		$A_P(m^2)$	T_1(℃)	$P_1(kPa)$	$I\ (\frac{W}{m^2})$	$V_{wt}\ (\frac{m}{s})$	η_{Turbine} (%)	Maximum η_{en}
Plan B	Optimization	5127	90.80	789.20	792.70	9.50	0.88	38.88
Plan C	Optimization	7028	99	414.1	481.5	9.14	0.99	32.88
		$A_P(m^2)$	T_1(℃)	$P_1(kPa)$	$I\ (\frac{W}{m^2})$	$V_{wt}\ (\frac{m}{s})$	η_{Turbine} (%)	Maximum η_{ex}
Plan B	Optimization	5775	92.21	654.2	628.1	9.16	0.99	38.25
Plan C	Optimization	7040	87.26	401.6	208	9.91	0.94	63.3
		$A_P(m^2)$	T_1(℃)	$P_1(kPa)$	$I\ (\frac{W}{m^2})$	$V_{wt}\ (\frac{m}{s})$	η_{Turbine} (%)	Minimum $\dot{Z}_K$ (\$/h)
Plan B	Optimization	7135	76.2	654.4	1200	2.83	0.94	41.01
Plan C	Optimization	10074	40.51	430.4	897.6	2.69	0.68	45

Table 9. The optimal value of multi-variable and multi-objective results for plan B and C.

		$A_P(m^2)$	T_1(℃)	$P_1(kPa)$	$I\ (\frac{W}{m^2})$	$V_{wt}\ (\frac{m}{s})$	η_{Turbine} (%)	η_{energy}	η_{exergy}	$\dot{Z}_K$ (\$/h)
Plan B	Base Case	10000	60.85	1200	800	5.5	0.85	18.81	8.37	61.4
	Optimization	10269	50.93	790.78	1196.1	5.74	0.75	20.6	8.45	59.90
Plan C	Base Case	10000	60.85	1200	800	5.5	0.85	10.76	7.14	59.51
	Optimization	9410.50	54.18	992.94	1273.20	5.69	0.99	11.2	6.65	58

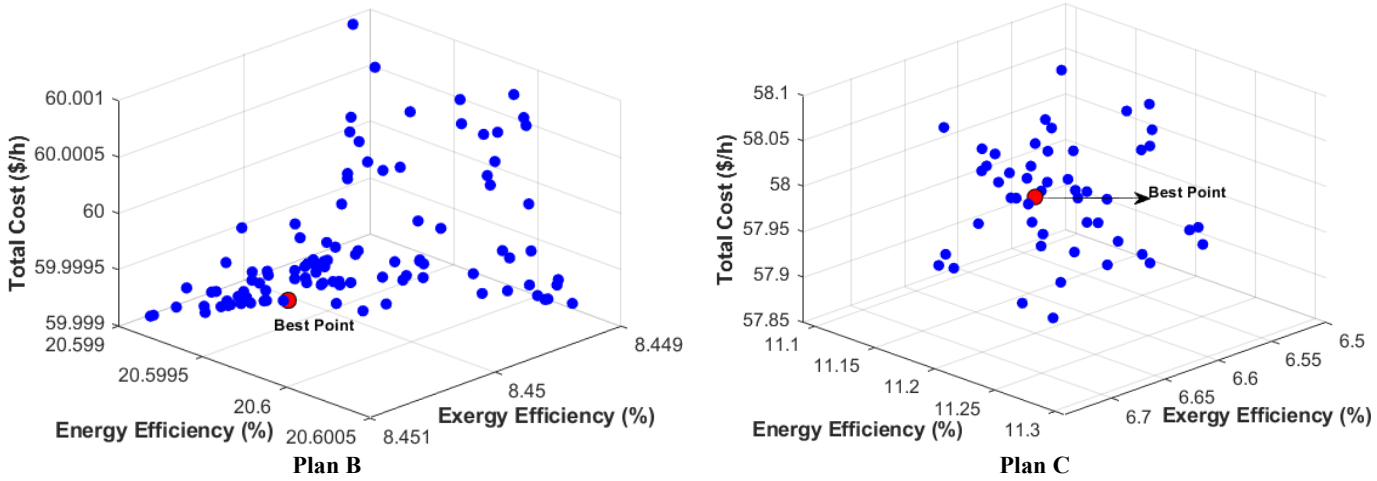

Figure 16. Pareto front of multi-objective optimization to display optimal distribution and data diversity.

7. Conclusion

This study evaluated the influence of various working fluids on the performance of two renewable energy systems:

- **Plan B**: A hybrid system integrating thermoelectric and wind turbine technologies
- **Plan C**: A wind turbine-only system

Machine learning (using Random Forest Regression) and NSGA-II multi-objective optimization were employed to predict and optimize system performance in terms of energy efficiency, exergy efficiency, and cost.

Key findings:

- **Working Fluid Performance**
  - *R227ea* demonstrated the best performance, with the highest energy efficiency (8.6%) and power output (433.5 kW), along with minimal exergy destruction.
  - *R125* showed the weakest performance, associated with the highest exergy destruction.
- **System Comparison**
  - *Plan B* consistently outperformed *Plan C* across all evaluated metrics, highlighting the advantages of hybrid system integration.
- **Optimization Insights**
  - The Pareto front analysis revealed clear trade-offs between efficiency and cost, with optimal conditions achieving up to 38% energy efficiency under multi-objective optimization.

The combination of optimal working fluid (R227ea) and a hybrid system design (Plan B) significantly enhances system performance and cost-effectiveness, providing a viable pathway toward more sustainable and efficient renewable energy systems.

8. ACKNOWLEDGEMENT

The authors are very grateful to the Hamedan University of Technology for supporting the project.

NOMENCLATURE

English signs

Heat transfer rate	$\dot{Q}(W)$
Electric power	$\dot{w}(W)$
Flow rate	$\dot{m}(\frac{kg}{s})$
Heat loss coefficient	F_R
Specific enthalpy	h$(\frac{kJ}{kg})$
Area	$A(m^2)$

Cost rate	$\dot{Z}(\frac{\$}{s})$
Energy produced by the solar collector	$\dot{Q}_U$
Overall collector loss coefficient	U_L
Heat transfer	$\dot{E}_X^Q$
Exergy work	$\dot{E}_X^W$
Physical exergy	ex_{ph}
Chemical exergy gas mixture	ex_{ch}
Irreversibility	$\dot{I}$
Pinch point evaporator	PP_{Eva}
Temperature sun	T_{Sun}
Thermoelectric work	$\dot{W}_{TEG}$
Specific entropy	$s(\frac{kJ}{kg})$
Exergy solar	E_{Sun}
Heat transfer evaporator	$\dot{Q}_{Eva}$
Greek signs	
Productivity	η
Working hour per year	hour
Fluid density	ρ
Lifetime of the power plant	n
Exergy efficiency	ψ
Maintenance coefficient	ϕ
Subscripts and superscripts	
Counter of components	K
Ambient condition	0
Cold	C
Warm	W

REFERENCES

1. Abbas, S. M., Alhassany, H. D. S., Vera, D., & Jurado, F. (2023). Review of enhancement for ocean thermal energy conversion system. *Journal of Ocean Engineering and Science*, *8*(5), 533-545. . https://doi.org/10.1016/j.joes.2022.03.008

2. Ahmadi, P., Dincer, I., & Rosen, M. A. (2013). Energy and exergy analyses of hydrogen production via solar-boosted ocean thermal energy conversion and PEM electrolysis. *International Journal of Hydrogen Energy*, *38*(4), 1795-1805. . https://doi.org/10.1016/j.ijhydene.2012.11.025

3. Akrami, E., Khazaee, I., & Gholami, A. (2018). Comprehensive analysis of a multi-generation energy system by using an energy-exergy methodology for hot water, cooling, power and hydrogen production. *Applied Thermal Engineering*, *129*, 995-1001. http://dx.doi.org/10.1016/j.applthermaleng.2017.10.095

4. Assareh, E., Assareh, M., Alirahmi, S. M., Jalilinasrabady, S., Dejdar, A., & Izadi, M. (2021). An extensive thermo-economic evaluation and optimization of an integrated system empowered by solar-wind-ocean energy converter for electricity generation–Case study: Bandar Abas, Iran. *Thermal Science and Engineering Progress*, *25*, 100965. https:/doi.org/10.1016/j.tsep.2021.100965

5. Assareh, E., Delpisheh, M., Alirahmi, S. M., Tafi, S., & Carvalho, M. (2022). Thermodynamic-economic optimization of a solar-powered combined energy system with desalination for electricity and freshwater production. *Smart Energy*, *5*, 100062. https:/doi.org/10.1016/j.segy.2021.100062

6. Atiz, A., Karakilcik, H., Erden, M., & Karakilcik, M. (2019). Assessment of electricity and hydrogen production performance of evacuated tube solar collectors. *International Journal of Hydrogen Energy*, *44*(27), 14137-14144. . https://doi.org/10.1016/j.ijhydene.2018.09.100

7. Bernardoni, C., Binotti, M., & Giostri, A. (2019). Techno-economic analysis of closed OTEC cycles for power generation. *Renewable Energy*, *132*, 1018-1033. https://doi.org/10.1016/j.renene.2018.08.007

8. Chen, W., & Huo, E. (2023). Opportunities and challenges of ocean thermal energy conversion technology. *Frontiers in Energy Research*, *11*, 1207062. https:/doi.org/10.3389/fenrg.2023.1207062

9. Delpisheh, M., Haghghi, M. A., Athari, H., & Mehrpooya, M. (2021). Desalinated water and hydrogen generation from seawater via a desalination unit and a low temperature electrolysis using a novel solar-based setup. *International Journal of Hydrogen Energy*, *46*(10), 7211-7229. https:/doi.org/10.1016/j.ijhydene.2020.11.215

10. Dezhdar, A., Assareh, E., Keykhah, S., Bedakhanian, A., & Lee, M. (2023). A transient model for clean electricity generation using Solar energy and ocean thermal energy conversion (OTEC)-case study: Karkheh dam-southwest Iran. *Energy Nexus*, *9*, 100176. https:/doi.org/10.1016/j.nexus.2023.100176

11. Geravandi, M., & Moradi CheshmehBeigi, H. (2022). The problem of resilient stochastic unit commitment with consideration of existing uncertainties using the rate of change of frequency. *Journal of Renewable Energy and Environment*, *9*(4), 34-47. https://doi.org/10.30501/jree.2022.306473.1262

12. Gong, J., Gao, T., & Li, G. (2013). Performance analysis of 15 kW closed cycle ocean thermal energy conversion system with different working fluids. *Journal of solar energy engineering*, *135*(2), 024501. https:/doi.org/10.1115/1.4007770

13. Habibollahzade, A., Gholamian, E., Ahmadi, P., & Behzadi, A. (2018). Multi-criteria optimization of an integrated energy system with thermoelectric generator, parabolic trough solar collector and electrolysis for hydrogen production. *International Journal of Hydrogen Energy*, *43*(31), 14140-14157. https:/doi.org/10.1016/j.ijhydene.2018.05.143

14. Hall, K., Kelly, S., & Henry, L. (2022). Site selection of ocean thermal energy conversion (OTEC) plants for barbados. *Renewable Energy*, *201*, 60-69. https:/doi.org/10.1016/j.renene.2022.11.049

15. Hoseinzadeh, S., Assareh, E., Riaz, A., Lee, M., & Garcia, D. A. (2023). Ocean thermal energy conversion (OTEC) system driven with solar-wind energy and thermoelectric based on thermo-economic analysis using multi-objective optimization technique. *Energy Reports*, *10*, 2982-3000. https://doi.org/10.1016/j.egyr.2023.09.131.

16. Hoseinzadeh, S., PaeinLamouki, M. A., & Garcia, D. A. (2024). Thermodynamic analysis of heat storage of ocean thermal energy conversion integrated with a two-stage turbine by thermal power plant condenser output water. *Journal of Energy Storage*, *84*, 110818. https:/doi.org/10.1016/j.est.2024.110818

17. Houshfar, E. (2020). Thermodynamic analysis and multi-criteria optimization of a waste-to-energy plant integrated with thermoelectric generator. *Energy Conversion and Management*, *205*, 112207. http://dx.doi.org/10.1016/j.enconman.2019.112207

18. Hu, F., & Wang, Z. (2023). Integration design and control strategy of sCO2 Brayton cycle for concentrated solar power system. *Energy Reports*, *9*, 2861-2868. https:/doi.org/10.1016/j.egyr.2023.01.111

19. Islam, M., Hassan, N., Rasul, M., Emami, K., & Chowdhury, A. A. (2022). Assessment of solar and wind energy potential in Far North Queensland, Australia. *Energy Reports*, *8*, 557-564. https:/doi.org/10.1016/j.egyr.2022.10.134

20. Jamil, I., Lucheng, H., Habib, S., Aurangzeb, M., Ahmed, E. M., & Jamil, R. (2023). Performance evaluation of solar power plants for excess energy based on energy production. *Energy Reports*, *9*, 1501-1534. https:/doi.org/10.1016/j.egyr.2022.12.081

21. Kannan, N., & Vakeesan, D. (2016). Solar energy for future world:-A review. *Renewable and sustainable energy reviews*, *62*, 1092-1105. https://doi.org/10.1016/j.rser.2016.05.022

22. Keshavarzzadeh, A. H., & Ahmadi, P. (2019). Multi-objective techno-economic optimization of a solar based integrated energy system using various optimization methods. *Energy Conversion and Management*, *196*, 196-210. https:/doi.org/10.1016/j.enconman.2019.05.061

23. Khosravi, A., Syri, S., Assad, M. E. H., & Malekan, M. (2019). Thermodynamic and economic analysis of a hybrid ocean thermal energy conversion/photovoltaic system with hydrogen-based energy storage system. *Energy*, *172*, 304-319. https:/doi.org/10.1016/j.energy.2019.01.100

24. Li, N., Dong, J., Liu, L., Li, H., & Yan, J. (2023). A novel EMD and causal convolutional network integrated with Transformer for ultra short-term wind power forecasting. *International Journal of Electrical Power & Energy Systems*, *154*, 109470. https:/doi.org/10.1016/j.ijepes.2023.109470

25. Liu, B.-T., Chien, K.-H., & Wang, C.-C. (2004). Effect of working fluids on organic Rankine cycle for waste heat recovery. *Energy*, *29*(8), 1207-1217. https:/doi.org/10.1016/j.energy.2004.01.004

26. Mao, L., Wei, C., Zeng, S., & Cai, M. (2023). Heat transfer mechanism of cold-water pipe in ocean thermal energy conversion system. *Energy*, *269*, 126857. https:/doi.org/10.1016/j.energy.2023.126857

27. Mehrpooya, M., Raeesi, M., Pourfayaz, F., & Delpisheh, M. (2021). Investigation of a hybrid solar thermochemical water-splitting hydrogen production cycle and coal-fueled molten carbonate fuel cell power plant. *Sustainable Energy Technologies and Assessments*, *47*, 101458. https:/doi.org/10.1016/j.seta.2021.101458

28. Moradi CheshmehBeigi, H., & Geravandi, M. (2023). Unit commitment risk evaluation considering load uncertainty and wind power. *Journal of Energy Management and Technology*, *7*(3), 134-141. https://doi.org/10.22109/jemt.2023.311870.1342

29. Mousavi, N., Mohebbi, M., & Teimouri, M. (2017). Identifying the most applicable renewable energy systems of Iran. *International Journal of Scientific and Technology Research*, *6*(30), 51-59. https://www.ijstr.org/final-print/mar2017/Identifying-The-Most-Applicable-Renewable-Energy-Systems-Of-Iran.pdf

30. Sahu, B. K. (2015). A study on global solar PV energy developments and policies with special focus on the top ten solar PV power producing countries. *Renewable and sustainable energy reviews*, *43*, 621-634. https:/doi.org/10.1016/j.rser.2014.11.058

31. Shahin, M. S., Orhan, M. F., Saka, K., Hamada, A. T., & Uygul, F. (2023). Energy assessment of an integrated hydrogen production system. *International Journal of Thermofluids*, *17*, 100262. https:/doi.org/10.1016/j.ijft.2022.100262

32. Sinama, F., Martins, M., Journoud, A., Marc, O., & Lucas, F. (2015). Thermodynamic analysis and optimization of a 10 MW OTEC Rankine cycle in Reunion Island with the equivalent Gibbs system method and generic optimization program GenOpt. *Applied Ocean Research*, *53*, 54-66. https:/doi.org/10.1016/j.apor.2015.07.006

33. Soto, R., & Vergara, J. (2014). Thermal power plant efficiency enhancement with Ocean Thermal Energy Conversion. *Applied thermal engineering*, *62*(1), 105-112. https:/doi.org/10.1016/j.applthermaleng.2013.09.025

34. Tsatsaronis, G., & Morosuk, T. (2008). A general exergy-based method for combining a cost analysis with an environmental impact analysis: Part II—application to a cogeneration system. *ASME International Mechanical Engineering Congress and Exposition*, , http://dx.doi.org/10.1115/IMECE2008-67219

35. Wang, E., Zhang, H., Fan, B., Ouyang, M., Zhao, Y., & Mu, Q. (2011). Study of working fluid selection of organic Rankine cycle (ORC) for engine waste heat recovery. *Energy*, *36*(5), 3406-3418. https:/doi.org/10.1016/j.energy.2011.03.041

36. Wang, M., Jing, R., Zhang, H., Meng, C., Li, N., & Zhao, Y. (2018). An innovative Organic Rankine Cycle (ORC) based Ocean Thermal Energy Conversion (OTEC) system with performance simulation and multi-objective optimization. *Applied thermal engineering*, *145*, 743-754. https:/doi.org/10.1016/j.applthermaleng.2018.09.075

37. Wang, S., & Hung, T. (2010). Renewable energy from the sea-organic Rankine Cycle using ocean thermal energy conversion. Proceedings of the international conference on energy and sustainable development: issues and strategies (ESD 2010), http://dx.doi.org/10.1109/ESD.2010.5598775

38. Wu, Z., Feng, H., Chen, L., Xie, Z., & Cai, C. (2019). Pumping power minimization of an evaporator in ocean thermal energy conversion system based on constructal theory. *Energy*, *181*, 974-984. https:/doi.org/10.1016/j.energy.2019.05.216

39. Yang, M.-H., & Yeh, R.-H. (2014). Analysis of optimization in an OTEC plant using organic Rankine cycle. *Renewable Energy*, *68*, 25-34. https:/doi.org/10.1016/j.renene.2014.01.029

40. Yang, M., Jiang, Y., Zhang, W., Li, Y., & Su, X. (2024). Short-term interval prediction strategy of photovoltaic power based on meteorological reconstruction with spatiotemporal correlation and multi-factor interval constraints. *Renewable Energy*, *237*, 121834. https:/doi.org/10.1016/j.renene.2024.121834

41. Yi, S., Zhang, Z., Peng, W., Zhang, J., & Yuan, H. (2022). Pre-expansion ejector absorption power cycle for ocean thermal energy conversion. *Energy Conversion and Management*, *269*, 116151. https:/doi.org/10.1016/j.enconman.2022.116151

42. Yoon, J.-I., Son, C.-H., Baek, S.-M., Kim, H.-J., & Lee, H.-S. (2014). Efficiency comparison of subcritical OTEC power cycle using various working fluids. *Heat and Mass Transfer*, *50*, 985-996. https://doi.org/10.1007/s00231-014-1310-8

43. Zheng, J., Liang, Z.-T., Li, Y., Li, Z., & Wu, Q.-H. (2024). Multi-agent reinforcement learning with privacy preservation for continuous double auction-based p2p energy trading. *IEEE Transactions on Industrial Informatics*, *20*(4), 6582-6590. https://www.researchgate.net/publication/364935917

44. Zhou, S., & Cao, S. (2022). Energy flexibility and viability enhancement for an ocean-energy-supported zero-emission office building with respect to both existing and advanced utility business models with dynamic responsive incentives. *Energy Reports*, *8*, 10244-10271. https:/doi.org/10.1016/j.egyr.2022.08.005